Extreme Mechanics Letters 74 (2025) 102277

Contents lists available at ScienceDirect

Extreme Mechanics Letters

journal homepage: www.elsevier.com/locate/eml

Fresh considerations regarding time-dependent elastomeric fracture

Shi-Qing Wang [*], Zehao Fan [1], Asal Siavoshani [1], Ming-chi Wang, Junpeng Wang

School of Polymer Science and Polymer Engineering, University of Akron, Akron, OH 44325, USA

ARTICLE INFO

Keywords:
Elastomeric fracture
Tensile strength
Toughness
Elastomeric rupture
Internal clock
Wg number

ABSTRACT

The fracture behavior of polymers in elastomeric state exhibits rich characteristics. Stretch rate and temperature can independently, as well as in combination, influence how such polymeric networks resist crack initiation and propagation. The strong rate and temperature dependencies of tensile strength and toughness in absence of high viscoelasticity, previously shown to occur in Rubber Chem&Tech **96**, 530, 2023 and plausibly in J. Polym. Sci. **18**, 189, 1955 and **32**, 99, 1958 are also observed in rate-sensitive elastomers. This work aims to propose, at a conceptual level, a general understanding of elastomeric fracture by addressing the considerable confusion surrounding the relationship between crack growth rate (v_c) and Griffith-Irwin's energy release rate (G_c) in different elastomeric systems. Our fracture tests demonstrate that (a) crack propagation velocity v_c varies with the applied loading level produced by either stepwise or continuous stretching, (b) emergent entanglement effectively modifies network structure and the relationship between v_c and G_c, and (c) temperature T affects v_c at a given load. We conclude that the magnitude of imposed strain, from which G_c may be evaluated, prescribes the level of bond tension in load-bearing network strands and dictates bond dissociation kinetics. Consequently, crack growth rate depends explicitly on loading level (e.g., G_c) and temperature. In the relationship between v_c and G_c, v_c is the effect and G_c is the cause, contrary to the previous viewpoint.

1. Introduction

Fracture of polymeric networks limits their applications and is therefore an important topic in materials engineering. Because of their extensive industrial applications including tires for automobiles and airplanes, study of fracture behavior of rubber vulcanizates has a long history of more than seven decades, following the Griffith-Irwin description [1,2] of fracture criterion. Unlike inorganic glasses that display brittle fracture at very small strains, elastomeric fracture [3] has presented some unique challenges, partially because of strong rate and temperature effects [4] and partially because of their high stretchability [5,6]. On the one hand, linear elastic fracture mechanics (LEFM) seemed hardly applicable. On the other hand, the pure-shear protocol [3] (involving a wide but short specimen) of Rivlin and Thomas has been effectively used [4,7–9] to characterize moderately stretchable polymer networks by evaluating the energy release rate.

It was discovered from the beginning [4] that different loads, expressed in terms of Griffith-Irwin's energy release rate G_c [1,2,10], would result in different values of crack propagation velocity v_c. The relationship between G_c and v_c can be readily demonstrated using either trouser tearing or peeling between two crosslinked elastomeric sheets to measure the required force F_c arising from tearing or peeling at a prescribed rate [4,9,11]. Here tearing energy or peeling energy, defined as $T_c = F_c/B$ or F_c/W, matches the dimension of G_c, where B is the sheet thickness in trouser tearing and W is the sheet width in a peeling test. Because the equivalence between G_c and T_c was suggested in the initial stage of development [7,12], tearing test is often carried out to show that G_c is dependent on crack propagation velocity v_c. In this interpretation, the tearing speed is regarded as indicating v_c. The phenomenology can be expressed as

$$G_c(v_c, T) = G_0[1+g(v_c A_T)], \tag{1}$$

where G_0 is the value of G_c in the long time or zero speed limit, the function g ($>> 1$) has been viewed as reflecting "viscous dissipation" [7,13] or viscoelastic processes [11,14,15]. Here A_T may resemble the WLF shift factor [16] $a_T = \tau(T)/\tau(T_{ref})$. The earliest form of Eq. (1) can be traced back to peeling tests [17–19] conducted at different rates and temperatures. In polymer physics, a_T is shown to depict temperature dependence of polymer dynamics, e.g., the dominant relaxation time τ that increases with decreasing T relative to a reference temperature T_{ref}

* Corresponding author.
E-mail address: swang@uakron.edu (S.-Q. Wang).
[1] Equal contribution.

https://doi.org/10.1016/j.eml.2024.102277
Received 18 July 2024; Received in revised form 8 December 2024; Accepted 9 December 2024
Available online 13 December 2024

> T. Moreover, polymers are known to show variation of mechanical (rheological) properties with experimental timescales, a feature known as viscoelasticity. However, when the response of stretching is purely elastic [20], the origin of the rate and temperature effects must be different from the explanation [7,11,14,15,21–24] based on linear viscoelasticity, which relates [11] G_c to frequency dependence of dynamic modulus G'. In the literature, Lake-Thomas model [25] is applied to estimate the prefactor G_0 by assuming such fracture to involve only one monolayer defined by a strand between adjacent crosslinks. In general, elastomeric fracture appears to involve an extensive region of high stress comparable to fracture strength according to recent spatial-temporal resolved polarized optical microscopic (*str*-POM) measurements [8,20,26] and modeling [27]. Considering fracture at an interface involving scission of chains bridging the two surfaces, Chaudhury [28,29] treated bond dissociation as an Eyring activation process and showed that the fracture energy G depends on the velocity V used to stretch the bridging chains as $G^{1/2} \sim lnV$.

Although the empirical expression Eq. (1) originated from tearing and peeling tests, pure shear tests also revealed a similar trend [9]. Instead of Eq. (1), it is more instructive to express the rate and temperature effects as

$$\nu_c A_T = g^{-1}(G_c/G_0 - 1), \tag{2}$$

where the magnitude of energy release rate G_c describes the loading level for either continuous or stepwise stretching of prenotched specimen or step stretch of notch-free specimen, followed by introduction of cut with a pair of scissors. Eq. (2) expresses the causality: higher G_c arising from a greater degree of stretching results in higher ν_c, which can be rationalized in terms of a recently proposed bond dissociation theory [30] for elastomeric rupture. Such causal reversal has also recently been recognized, attributing fracture to chain scission [31–34]. The dependence of ν_c on G_c is characteristically exponential. As shown in Section 4.2, ν_c is highly (exponentially) dependent on the state of stretching, from which G_c may be evaluated. In other words, it is logically more accurate to rewrite Eq. (2) and show that ν_c is an increasing function of the imposed load, e.g., the level of stretching.

Since the energy-based approach of Griffith-Irwin does not characterize fracture in terms of ν_c it has been challenging to describe elastomeric fracture that follows either Eqs. (1) or (2). Consequently, there has not been any satisfactory explanation for how and why fracture (1) occurs at a higher ν_c for a higher value of G_c and (2) displays different values of ν_c at different temperatures for a given G_c. In pure shear tests Rivlin-Thomas formula

$$G_c = w(\lambda_c)h_0 \tag{3}$$

can be employed to measure G_c at different values of stretch rate $\dot{\lambda} = V/h_0$, where V is the crosshead speed and h_0 is the sample's initial height [20,35]. Here higher stretch rate in prenotched pure shear can push the onset of fracture to higher strain and corresponding higher G_c, leading to faster crack growth because higher bond tension leads to short bond lifetime [30]. Consequently, although pure shear tests in continuous stretching do not directly control and prescribe crack propagation velocity, ν_c can be expected to increase with applied rate $\dot{\lambda}$ from which a corresponding G_c emerges.

An elastomer may or may not contain entanglement that is due to mutual chain uncrossability among long strands between crosslinkers. Even when it does, depending on the magnitude of stretch rate, entanglement may not emerge to affect stress response and fracture behavior. In this work we study three types of elastomers, one showing the entanglement effect, so that stress-strain curves do not overlap at different rates, and the other two showing no sign of rate dependence. According to basic principles of polymer rheology, entanglement in vulcanized networks can lead to significantly higher stress responses, as found to be the case for VHB4910 (3 M acrylic polymer-based elastomer). Conversely, in absence of entanglement contribution to stress, stress vs. strain curves overlap in a wide range of stretch rate while exhibiting higher tensile strength at higher rate [20]. This is the case for the present vulcanized styrene-butadiene rubber (SBR) and crosslinked poly(methyl acrylate) (PMA).

To avoid confusion, it is imperative to clarify at the outset the important terminology used in this work relative to how it is used in literature on elastomeric rupture and fracture, i.e., phrases such as (a) *viscoelasticity*, (b) *viscous or plastic process* and (c) *energy dissipation*. (a) Meaning of being viscoelastic: Materials such as elastomers can be *viscoelastic* because their (elastic) structures can be dynamic and undergo rearrangement on their own timescales. Even in the simplest description, based on a single dominant relaxation time τ, stress response could become rate depependent if τ matches the external timescale, on which the elastomer is stretched. Specifically, when its transient structures such as embedded entanglement (due to chain uncrossability) are mechanically deformed within their relaxation time, the *elastic* response is rate dependent, stronger (involving higher stress) at faster stretching. This rate dependence is frequently regarded to be viscoelastic in origin although the stress response may be fully elastic, free of any contribution from viscous flow. Elastomers with embedded topological entanglement turns purely elastic (rather than viscoelastic) at high temperatures where the "lifetime" of such entanglement, τ, is vanishingly short relative to the reciprocal stretch rate. With such effectively slow stretching, only the permanent elastic structure formed by load-bearing strands between crosslinks survive. In contrast, a viscoelastic liquid flows like a Newtonian liquid on long timescales. In passing, it is noted that a viscoelastic *liquid* is only elastic during initial deformation, which is captured by Maxwell model. Most viscoelastic materials exhibit initial response to startup deformation in such a Maxwellian manner, i.e., do not obey Kelvin-Voigt model. Boger like fluids [36], e.g., dilute viscous solution of polymers are an exception. (b) Meaning of being viscous or plastic: Viscous or plastic processes are irreversible, involving irrecoverable deformation. Thus, being viscous is entirely different from the concept of viscoelasticity whose description, as commented in (a), involves comparison of Maxwell-like relaxation time with stretch rate. Unless it is close to the glass transition temperature T_g, viscous stress is negligible in comparison to elastic stress arising from elastomeric stretching. Upon lowering temperature toward T_g intersegment interactions can lead to formation of another short-ranged elastic structure with a finite relaxation time [37]. Upon external deformation, this structure will yield and break down, resulting in a dissipative structure that produces a viscous stress. Discussion of this low temperature transient elastic and high viscous behavior associated with intersegmental interactions is beyond the scope of the present work and belongs to our future research. (c) Meaning of energy dissipation seems different in Griffith-Irwin's fracture mechanics from that used in physics. On the other hand, the usual concept of dissipation also motivated researchers to explain [9,38,39] why toughness decreases upon swelling elastomers with solvent that reduced loss modulus. Only elastic energy may be stored and released without loss. Energy in the form of entropic changes in the Helmholtz free energy can be stored during stretching and is only partially recoverable upon unloading when embedded entanglement makes additional contribution to the elastic stress buildup during stretching. A more specific discussion on this concept is presented below in Section 4.9.

In the literature, whenever toughness G_c is many decades larger than [3] surface free energy Γ, "energy dissipation" [7,9,13,40–44] is said to be involved in fracture. This is inevitable when adopting the traditional Griffith-Irwin energy-based description, which cannot prescribe any characteristic length scale for the fracture process. It is thus common to characterize elastomeric fracture as viscoelastic and dissipative, regardless of what processes are involved, either elastic, or viscoelastic, or viscous, or bond breaking, or disentangling, or frictional etc. Such a characterization can be confusing for elastomers under purely elastic stretching because the energy release rate G evaluated just before fracture is of the same magnitude as G_c and involves no viscous dissipation.

In this Review Article, we carry out pure shear experiments to elucidate crack growth under various loading conditions, from continuous stretching and stepwise stretching of prenotched specimens to preloading without prenotch before introducing a cut. In terms of temperature-dependent kinetics of bond dissociation [30], we can explain rate and temperature effects on elastomeric fracture, phenomena extensively reported and studied in the past seven decades. Faster crack growth, i.e., chain scission on shorter timescales, requires a higher degree of network stretching and thus correspondingly higher fracture toughness G_c. When the stretching is entirely elastic, higher G_c at higher crack propagation speed arises from the necessary higher degree of network stretching and is not due to viscous energy dissipation, a conclusion that has often been drawn in the energy-based Griffith style description of elastomeric fracture in the polymer literature [45,46]. This paper aims to discuss the origin of the relationship between G_c and v_c and is organized as follows. We present five different pure-shear-based experiments using three different elastomers in Sections 2 and 3. The objective of these experiments is to present two pieces of information. First, pure shear experiments carried out with different imposed stretch rates do not pre-determine crack propagation speed v_c and the corresponding energy release rate G_c. Second, rate and temperature effects on fracture still occur in absence of viscoelastic effects, e.g., without engagement of polymer entanglement. A comprehensive discussion in Section 4 follows where we discuss an exhaustive list of topics related to interpretations of the current experimental results and past explanations concerning the essence of elastomeric fracture. We (1) clarify concepts such as viscoelasticity and energy dissipation, (2) review the recently proposed theory for elastomeric fracture, (3) suggest bond-dissociation-controlled network lifetime as the internal clock to measure against the experimental timescale, and (4) question the meaning of past WLF like shifts to describe temperature dependence of tensile strength and toughness. We conclude in Section 5.

2. Rate dependent stretching: emergence of entanglement in VHB

Because of moderate crosslinking and relatively sluggish chain dynamics in VHB4910, embedded entanglement can readily emerge upon high rates of stretching. The purpose of choosing VHB4910 is to demonstrate that a leading effect of viscoelasticity is the contribution of entanglement, not viscous dissipation. This section focuses on the relationship between crack growth and imposed load, specified in both continuous and stepwise stretching by the stretch ratio or energy release rate estimated from Rivlin-Thomas formulation [3] of pure shear.

2.1. Continuous stretching

In the pure shear configuration, there are at least three ways to explore the relationship between crack propagation velocity v_c and the load, expressed in terms of either the stretch ratio h/h_0 or energy release rate G_c of Eq. (3). One is to apply continuous stretching until crack starts to propagate at a high velocity v_c at different values of stretch rate $\dot{\lambda} = V/h_0$. Fig. 1(a) shows the rising stress as a function of stretch ratio h/h_0 at four crosshead velocities (V), where the last data points mark the onset of fast fracture at $t_f = 4.4$, 42, 370 and 2970 s, corresponding to $\lambda_f = h_f/h_0$ equal to 4.7, 4.5, 4.1 and 3.5 respectively. In Supplementary Material (SM) we show in Fig. S1(a)-(b) that at a higher applied rate $\dot{\lambda}$ leads to proportional increases in birefringence and stress. There is a negligible

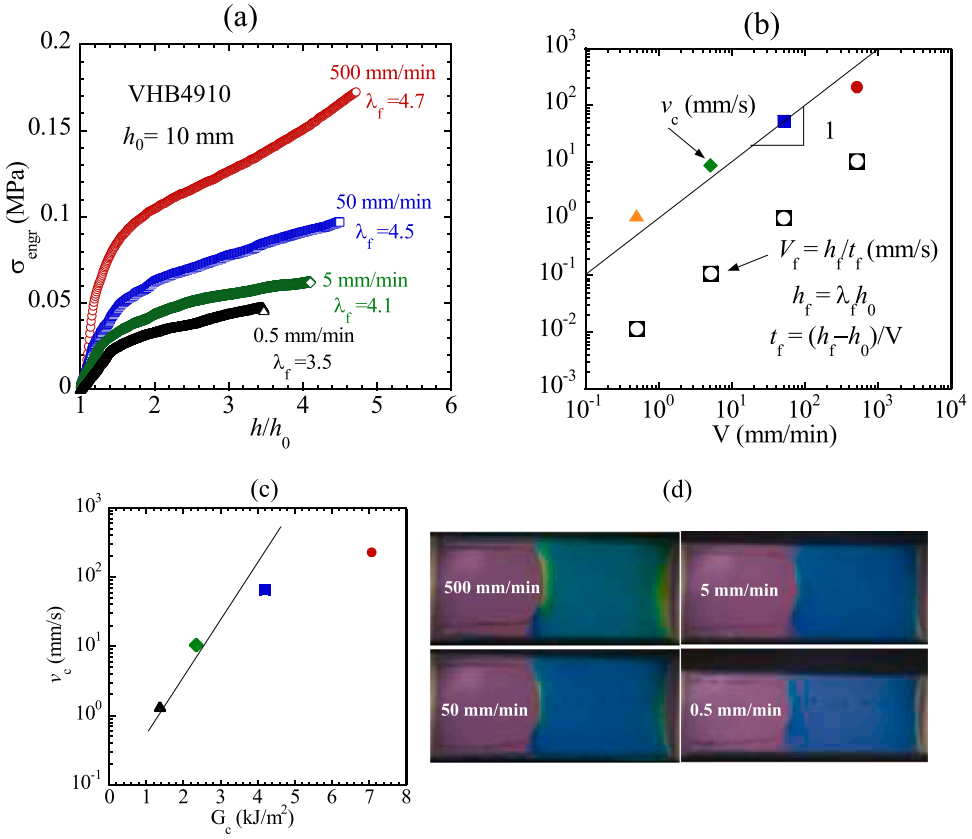

Fig. 1. Engineering stress vs. stretch ratio curves from continuous stretching of VHB4910 in pure shear at four crosshead speeds of V = 0.5, 5, 50 and 500 mm/min, where the last data points at $\lambda_f = h_f/h_0$ mark the onset of fast crack propagation. Prenotched specimens have dimensions of $h_0 = 10$ mm, W = 100 mm, thickness of 1 mm, and c = 30 mm. (b) Crack tip propagation velocity v_c at the four corresponding stretching velocity V, where the open symbols represent a velocity comparable to V. (c) The four crack propagation velocity as a function of the load level, given by Eq. (3). (d) Tip birefringence field at the four speeds just before the fast crack propagation with v_c given in (b) and (c).

viscous component of stress, and embedded entanglement in VHB4910 makes the sample undergo stronger elastic stretching. Because of the emergent entanglement at higher rates, fracture ended up taking place at comparable stretch ratio λ_f as shown in Fig. 1(a). Likewise, rupture of notch-free VHB takes place at comparable stretch ratios, as shown Fig. S1(a) in SM. Specifically, at higher rates the shorter elapsed time t_f is due to the emergence of entanglement that leads to more effective buildup of bond tension in load-bearing strands. In other words, in absence of entanglement, e.g., at sufficiently high temperatures, VHB4910 is simply weaker and less tougher, as expected from our theory of bond dissociation for fracture.

In general, a higher fracture load resulting from higher $\dot{\lambda}$ produces higher v_c, as shown by solid symbols in Fig. 1(b), i.e. the crack growth rate v_c almost linearly increases with imposed stretching speed V. The linearity between V_f and V shown in the open symbol suggests that pure shear tests of controlled rate $\dot{\lambda}$ have succeeded in prescribing the experimental timescale on which fracture occurs, corresponding to a certain level of bond tension. In the range of V from 500 to 0.5 mm/min a higher value of v_c (shorter timescale) is associated with higher energy release rate G_c, as shown in Fig. 1(c). At a higher V, (a) more entanglement participates in the network stretching, (b) the stretching duration is shorter before fracture presumably because there is higher bond tension buildup due to the emergence of more entanglement, leading to higher value of G_c (c) the higher stress response may involve higher chain tension. Moreover, as shown by extracted images from video recording in Fig. 1(d), the higher load level is accompanied by higher birefringence at notch tip. Video recordings also permit us to verify that the condition of pure shear holds during the continuous stretching, i.e., the space between adjacent marks remains essentially unchanged, e.g., see Movie-VHB50 for V = 50 mm/min in SM. Such recording also enables us to show a sudden slow-fast transition in crack propagation speed, which can jump by nearly two decades [47]. Fig. 1(b) only shows v_c on the fast branch.

2.2. Fracture at various stretch ratios: a case of preload

Instead of continuous stretching carried out in the preceding section, two more protocols can be used to apply different load levels and produce different values for v_c. For example, notch-free specimens can be first stretched to prescribed stretch ratios, followed by the introduction of a large cut to initialize fracture. This preload can be performed at various chosen stretch rates. Fig. 2(a) shows five discrete preloads produced with V = 500 mm/min to various stretch ratios from 3.5 to 7. Also shown in Fig. 2(a) is a stress vs. strain curve produced with V = 5 mm/min to $h/h_0 = 7$, where the stretching time is rescaled by a factor of 100 to fit on the same time scale. The difference between the two curves (red circles and purple line) reveals the same rate dependence of the stress responses as shown in Fig. S1 (a) in SM.

Fracture occurs upon cutting with a pair of surgeon's scissors before stress relaxation is complete (which takes a few hundred seconds), i.e., within a couple of seconds after step stretch. Fig. 2(b) shows in open circles the crack growth to be faster at higher stretch ratio, i.e., v_c increasing exponentially with h/h_0. When the much lower rate $\dot{\lambda}$ is applied to make the step stretch along the purple curve in Fig. 2(a), the loading condition approaches zero-rate limit. The crack growth is systematically slower, as shown by the difference between open circles and open squares. Both open symbols in Fig. 2(b) show v_c to increase with stretch ratio, from which G_c may be evaluated using Eq. (3) for either V = 500 or 5 mm/min, corroborating with Eq. (2). Also plotted in Fig. 2(b) are solid squares that are the same four solid data points from Fig. 1(b). Additionally, the solid circles represent the observations of fast crack growth from stepwise stretching of prenotched specimens to the various stretch ratios made with V = 50 mm/min. We see that two solid symbols converge to the open square at the lowest ratio of 3.5, at which crack growth takes place long after entanglement has relaxed. Conversely at 4.5, the solid circle catches up to the curve formed by open circles, where stress has little time to relax. Clearly, the transient presence of entanglement affects the crack growth rate.

3. Fracture behavior of SBR and PMA in absence of entanglement

When stress response shows no rate dependence, i.e., when stress vs. strain curves of notch-free elastomers overlap up to rupture, we may regard them to be entanglement-free. As shown before [20], in a wide temperature range from 30 °C to −10 °C (cf. Fig. 8(a) in Section 4.7) the vulcanized styrene-butadiene rubber (0.3phrSBR) shows no rate dependence in its stress vs. strain (SS) curves. Similarly, crosslinked poly (methyl acrylate) (xPMA) synthesized using a solution based method can show overlapping SS curves at different rates at room temperatures [48], implying little embedded entanglement. We show in this section that rate and temperature effects still take place in SBR and xPMA. Thus, as discussed in Section 4, these effects must have a different origin from polymer viscoelasticity.

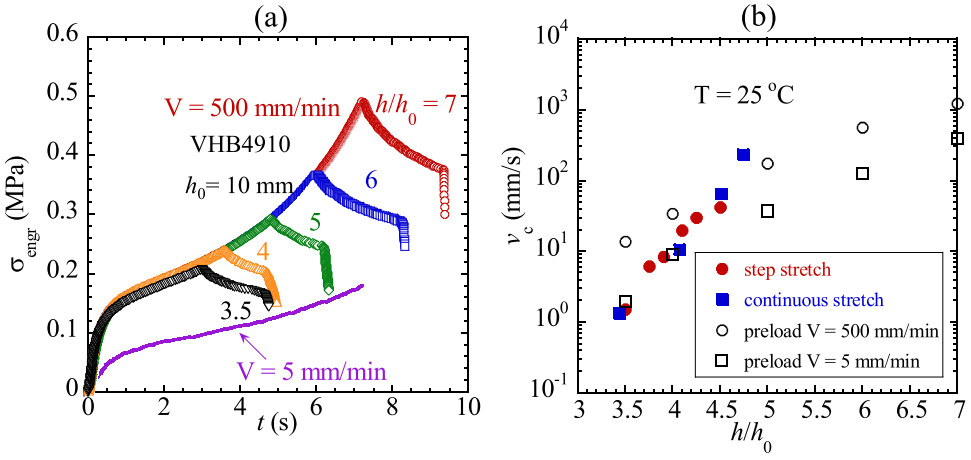

Fig. 2. (a) Engineering stress vs. time from step stretch of notch-free VHB4910 in pure shear to various stretch ratio, ranging from 3.5 to 7, followed by cutting within a couple of seconds. Also plotted is the stress vs. rescaled time curve produced by a much lower stretching speed of 5 mm/min instead of 500 mm/min. Specimens have dimensions of $h_0 = 10$ mm, W = 100 mm, thickness of 1 mm. (b) Crack propagation velocity v_c, following the cutting at the different stretching ratios produced by either high or low stretching speed, given by open circles and squares respectively. Also plotted are the four data from Fig. 1(b) in squares. Solid circles present results from stepwise stretching to the various stretch ratios of prenotched VHB4910 in pure shear.

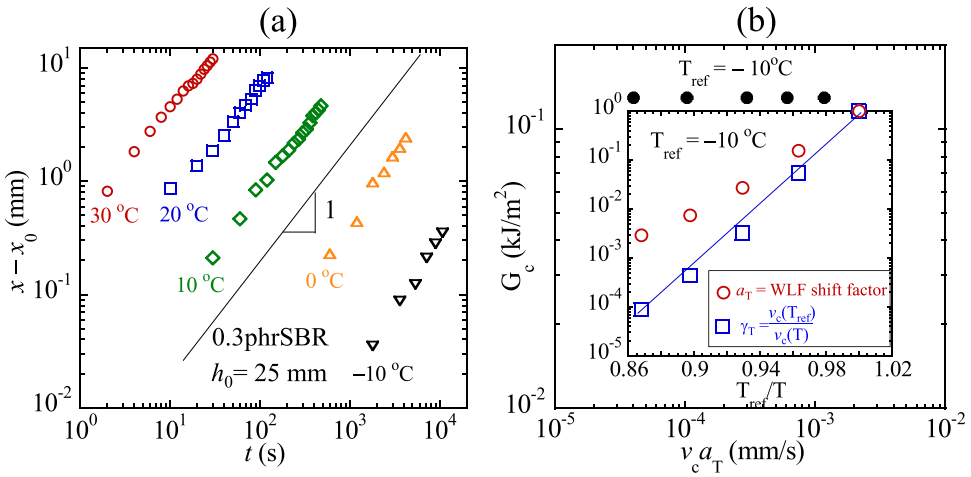

Fig. 3. (a) Notch tip displacement of SBR in pure shear as a function of time at five temperatures ranging from 30 to −10 °C to display four decades of variation, at a common load, corresponding to 5 % of stepwise stretching. (b) Toughness G_c plotted against the rescaled crack propagation velocity $v_c a_T$, where the inset figure shows how the normalized v_c changes with temperature, against the plot of the WLF shift factor a_T against temperature.

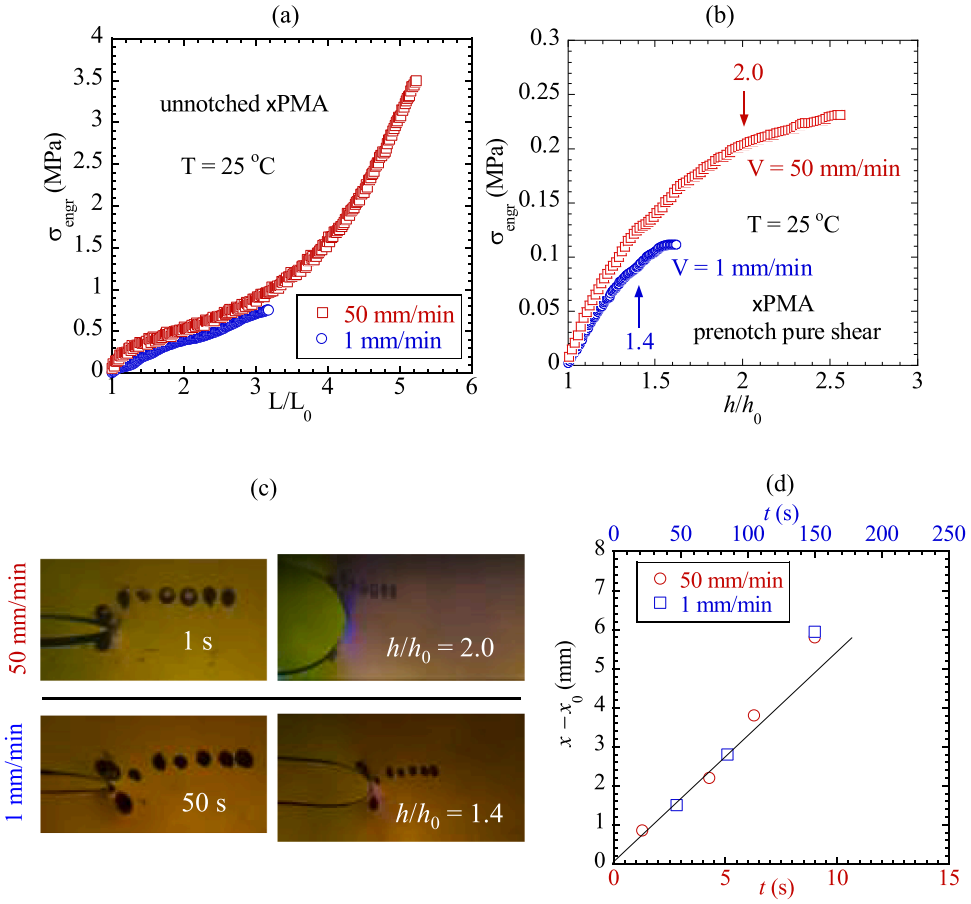

Fig. 4. (a) Engineering stress vs. stretch ratio from uniaxial extension of dogbone-shaped xPMA specimens at two crosshead speeds V = 1 and 50 mm/min, where the dogbone-shaped specimens were cut using ASTM D638 (type V) die. (b) Engineering stress vs stretch ratio curve from continuous stretching of prenotched xPMA in pure shear. Prenotched specimens have dimensions of h_0 = 10 mm, W = 60 mm, thickness of 1 mm, and c = 24 mm. Fracture occurs at h/h_0 = 1.4 and 2.0 respectively. (c) Images from video recording of the two tests shown in (b), at the beginning of stretching (left two images) and at onset of fracture (right two images). (d) Displacement of notch tip as a function of time for both rates, presented on double X axes, revealing v_c = 0.032 and 0.55 mm/s respectively.

3.1. Temperature dependence of crack growth for a common load (SBR) – stepwise stretch

One of the challenges to Griffith-Irwin style account of fracture is to explain how and why temperature can influence characteristics such as crack propagation velocity v_c(T) at a given load. Since few studies directly investigated such a case [47], we demonstrate it here using stepwise stretch in pure shear without any rate dependence of stress response that may arise from entanglement as shown in Section 2. At a fixed step-stretch ratio and therefore at the same G_c, we can explore

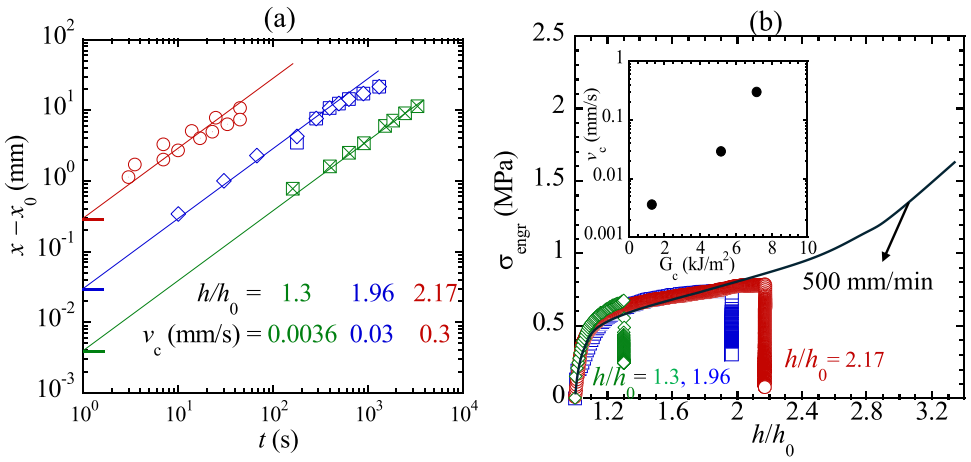

Fig. 5. (a) Notch tip displacement of SBR in pure shear as a function of time after three stepwise stretching to $h/h_0 = 1.3$, 1.96 and 2.17, at V = 10 mm/min. Prenotched specimens have dimensions of $h_0 = 10$ mm, W = 60 mm, thickness of 1 mm, and c = 24 mm. Circles correspond to measurements of crack growth 0 s after reaching 2.17 whereas the dotted circles are the data collected 8 s after the stepwise stretch. Squares correspond to measurements 0 s after reaching 1.96 whereas the diamonds show results collected 14 s after the stepwise stretch. (b) Engineering stress vs stretch ratio curves from three stepwise stretching of prenotched xPMA in pure shear. The line denotes the stress vs. strain curve of notch-free xPMA undergoing continuous stretching in pure shear. The inset shows a stronger than linear dependence of log(v_c) on load G_c.

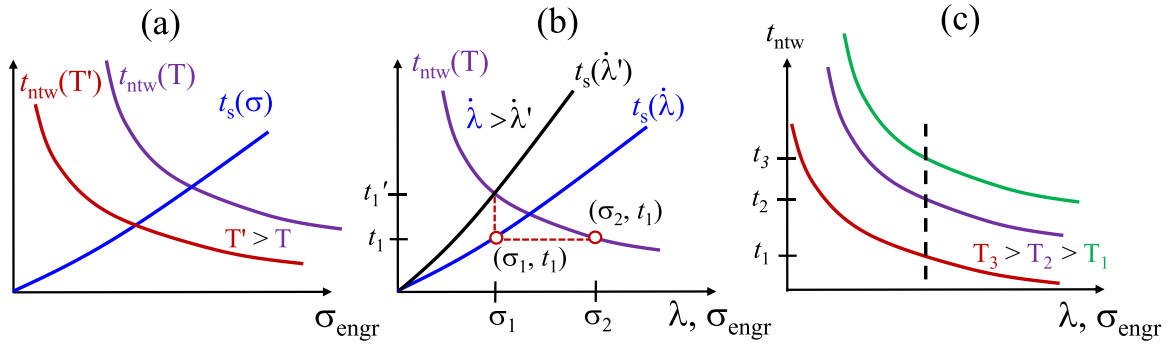

Fig. 6. (a) Qualitative sketch of stress dependence of network lifetime and increase of stretching time t_s with increasing stress. (b) Stretching time at two different stretch rates. At higher rate it takes a shorter time t_1 to arrive at a common stress σ_1 or stretch ratio where the lifetime well exceeds t_s, permitting further stretching. (c) Network lifetime as a function of stress at three temperatures, showing three values t_1, t_2 and t_3 at the same applied strain or stress, indicated by the vertical line.

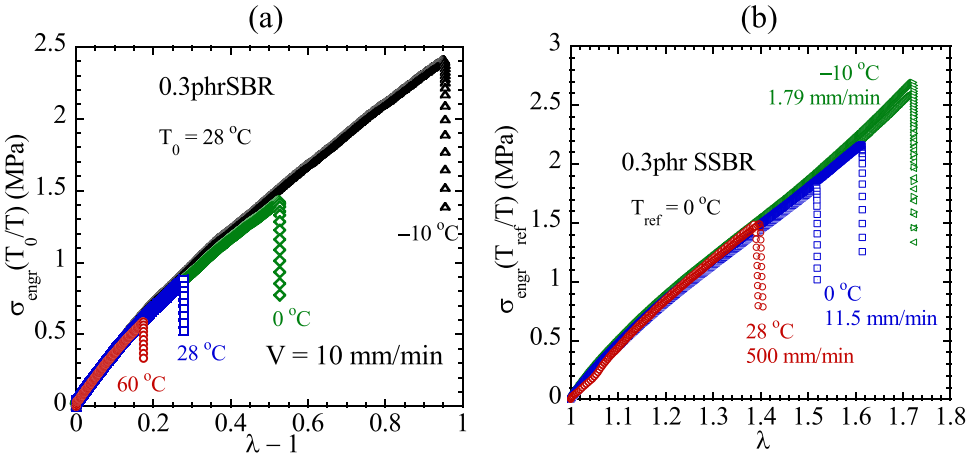

Fig. 7. (a) Engineering stress vs. stretch ratio from startup continuous stretching at a common crosshead speed V = 10 mm/min of dogbone shaped specimens that are prepared using ASTM D638 (type V) die, with the initial separation of upper and lower clamps given by $L_0 = 27$ mm. (b) Engineering stress vs. stretch ratio from startup continuous stretching at three temperatures at the effective stretch rate $\dot\lambda a_T$ equal to $V/L_0 = 0.43$ min^{-1} at $T_{ref} = 0$ °C.

whether v_c follows polymer dynamics described by the WLF shift factor a_T. In pure shear, the specimen's dimension is 25 × 100 × 1 mm^3 with a cut length of $a = 30$ mm. Stepwise stretching is made with crosshead speed V = 100 mm/min to a stretch ratio of $h/h_0 = 1.05$, reaching the same nominal stress level, independent of temperature, corresponding to $G_c = 0.13$ kJ/m^2. By video-recording the crack tip displacement over

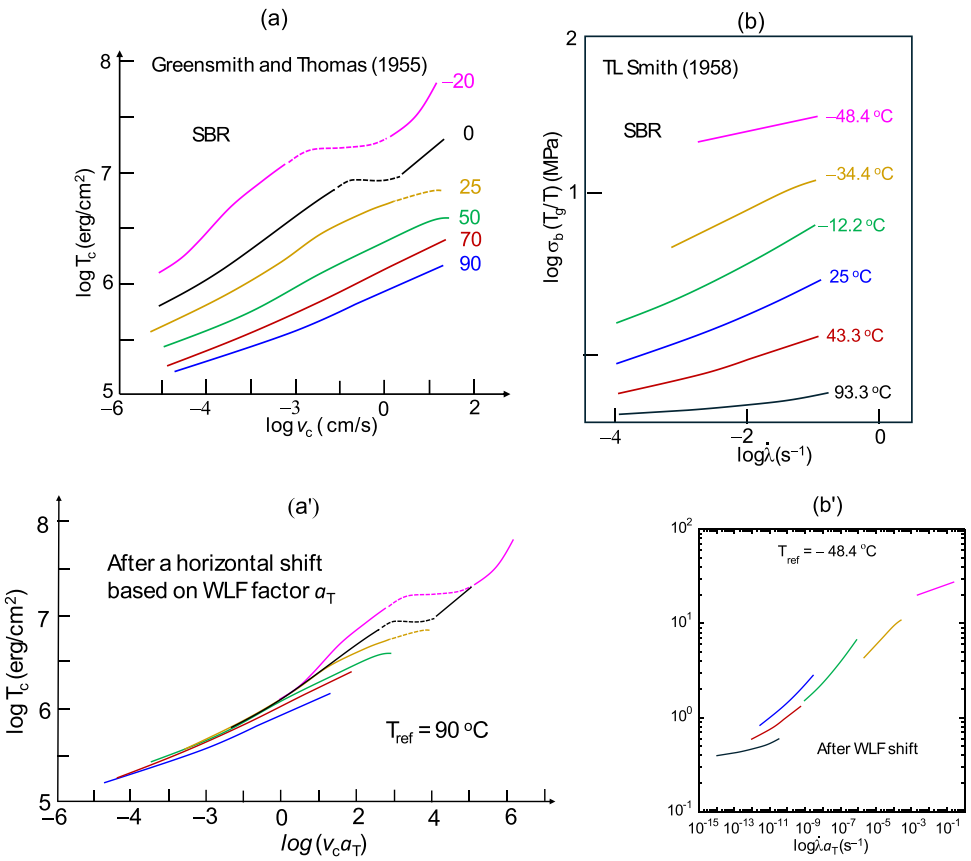

Fig. 8. (a) Tearing energy T_c required to make tearing at speed v_c in a range of temperature from 90 to −20 °C, from Greensmith-Thomas [4]. (b) Tensile strength as a function of stretch rate $\dot{\lambda}$ in a range of temperature from 93 to −48 °C, from Smith [66], reproduced by Kinloch in Fig. 10.10(a) of his book [45]. (a′) Horizontal shifts of curves in (a) to match the curve at T_{ref} = 90 °C. (b′) Shifts of curves in (b) according to the WLF shift factor a_T with at T_{ref} = −48.4 °C, which differs from the Fig. 10.10(b) in Kinloch's book. In other words, when the actual WLF factor a_T is used, the resulting curves do not overlap.

time at these temperatures, we can measure crack growth rate as shown in Fig. 3(a). See Movie-SBR20C for the test at 20 °C in SM. The temperature dependence of the velocity v_c(T) can be straightforwardly expressed in terms of a new shift factor γ_T defined as the ratio of the reciprocal v_c at temperature T to that at reference temperature T_{ref}. For example, the inset figure in Fig. 3(b) shows our shift factor γ_T as a function of T_{ref}/T, along with the WLF factor a_T. Here γ_T is obtained by plotting data in Fig. 3(a) against the rescaled time, i.e., against t/γ_T, so that all data would collapse onto one line.

Fig. 3(b) shows that Eq. (1) with $A_T = a_T$ did not hold: For a constant G_c, the product $v_c a_T$ should also have been a single value, i.e., a point in Fig. 3(b). Instead, the five data points spread over nearly two decades. Clearly, the correlation between G_c and v_c does not follow Eq. (1), which says that G_c is a function of $v_c A_T$ and A_T is the WLF shift factor a_T.

3.2. Continuous stretching of xPMA

Fig. 4(a) shows xPMA to be much stronger, displaying much stronger strain hardening at V = 100 mm/min and rupturing at higher stretch ratio and tensile strength σ_b = 3.5 MPa instead of 0.7 MPa at V = 1 mm/mm. In other words, elastomeric strength is rate dependent.

According to the recently uncovered relationship between toughness and material strength [26,30], we can expect this xPMA to be tougher at higher stretch rates. This is indeed the case, as shown Fig. 4(b). As in the case of notch-free stretching, the stress level at fracture does depend on the applied rate: fracture occurs at $h/h_0 = 1.4$, corresponding to time $t_f(1) = 0.4h_0/V(1)$, and that at $h/h_0 = 2$ involves a time $t_f(100) = h_0/V(50)$. Consequently $t_f(1)/t_f(50) = 0.4 \times 50 = 20$. Fig. 4(c) presents a panel of images at the beginning of stretching and at onset of fracture, extracted from Movie-PMA-CS1 and Movie-PMA-CS50. Fig. 4(d) shows the displacements of notch tip as a function of time at the two imposed crosshead speeds. The crack propagation velocity v_c is given by the slopes of the straight line in Fig. 4(d) that shows v_c = 0.032 and 0.55 mm/s, displaying a ratio of 17, remarkably close to the time ratio of 20, indicated above. The difference in v_c correlates with that in loading level G_c, which may be traced to the fact that the faster stretching prescribes a shorter timescale, permitting xPMA to undergo more stretching and stress buildup before fracture. The two images labeled by $h/h_0 = 2$ and 1.4 indicate higher birefringence at notch tip at 50 mm/min, consistent with the notion that elastomeric strength is not constant.

3.3. Stepwise stretching of xPMA

Fig. 1(c) appears to suggest an approximate exponential dependence of crack growth rate on the load, e.g., G_c. Before discussing the implications of such strong dependence in the next section, we further demonstrate this relationship based on a second batch of xPMA that has a slightly higher T_g. At crosshead velocity V = 100 mm/min, xPMA is respectively stepwise stretched to h/h_0 = 1.3, 1.96 and 2.17. Crack propagation velocity is measured from video recordings of these stepwise stretching tests. See Movie-PMA-SS2.2 in SM for the case of h/h_0 = 2.17. Fig. 5(a) shows the crack movements as a function of time upon these three stepwise stretching tests that produce the stress responses shown in Fig. 5(b) in three open symbols. Evaluating G_c according to Eq. (3), the inset in Fig. 5(b) shows an exponential increase of v_c with G_c, like Fig. 1(c)

4. Discussions

4.1. Polymer viscoelasticity

Respective influences of rate and temperature on characteristics of elastomeric fracture suggest that there are internal timescales. The experimental timescale, e.g., rate, measures against the internal clock. For seven decades, polymer relaxation time has been taken as the clock governing fracture processes. In other words, viscoelasticity has been considered [11,14,15,21–24,49] to play a dominant role in rate- and temperature-dependent elastomeric fracture. This Maxwell clock probably came about because a relationship between G_c and v_c in Eq. (1) has been explored in experiments to involve a *WLF like* shift factor A_T. In contrast, as briefly reviewed in Section 4.2 below, we have recently proposed [30] that the timekeeper is the network lifetime t_{ntw}, which can be expected to be shorter under a greater degree of stretching and at a higher temperature. Currently, a molecular model for t_{ntw} has yet to be developed because the relationship between bond lifetime t_b of Eq. (4), given below, and t_{ntw} depends on the network structure, which is generally unknown. In the present work, we assume that t_{ntw} may vary like t_b with respect to variables such as strain (stretch ratio) and temperature. The network reaches its lifetime when sufficient bond dissociation events have caused a macroscopic disconnection to separate an elastomer into two pieces. The fracture plane consists of a collective set of dissociating bonds. The dissociation forms a percolative three-dimensional fracture path and defines the network lifetime. Individual bond dissociation is clearly the triggering event. Conceivably, t_{ntw} may be orders of magnitude longer than t_b, making it invalid to draw conclusion made in Ref. [30] regarding its Fig. 16(b). While polymer relaxation time τ is a molecular parameter, t_{ntw} is a structural quantity, involving many chains, and may vary for the same elastomer from a notch-free system to a prenotched specimen with different crack tip geometries.

Progressively higher stress in higher rate stretching, as shown in Fig. 1(a) and S1(a) in SM, was usually regarded to imply that there is significantly morebulk energy dissipation. *In situ* birefringence measurements show in Fig. S1(b) that the higher stress is accompanied by proportionally higher birefringence. Apparently, (a) high-rate stretching enlists entanglement contributions to stress in VHB, (b) there is no viscous contribution to stress and (c) the low-rate stretching or high temperature stretching hardly engages any entanglement, as shown in Fig. S2. VHB shows stronger "strain hardening" through non-Gaussian chain stretching at higher rates. In other words, higher stress at higher rates, as shown in Fig. 1(a) or Fig. S1(a), partly stems from the stronger strain hardening due to a larger entanglement effect. However, the nature of stress is elastic, free of any viscous stress and corresponding energy dissipation.

Elastomers can be free of the so-called viscoelastic effects, e.g., stress vs. strain curves overlap before rupture, when examined well above the glass transition temperature T_g where entanglement relaxes on timescales much shorter than the reciprocal stretch rate. In this limit, which involves a large fraction of experimental data in the literature, e.g., plausibly data collected in the temperature range of from 90 °C to room temperature in Fig. 8(a)-(b) in Section 4.7, kinetics of bond dissociation completely dictates the rate and temperature dependence of toughness and tensile strength. At lower temperatures, rate-dependent rheological effects may occur in one of the following three distinct forms. First, the relaxation time of network strands becomes long enough relative to the imposed stretch rate $\dot{\varepsilon}$ so that tensions in load-bearing strands may increase with $\dot{\varepsilon}$. Using a simple scaling model that assigns a relaxation time τ_s to load-bearing network strands, we can suggest that at $\dot{\varepsilon} > 1/\tau_s$, i.e., for $Wi_s = \dot{\varepsilon}\tau_s > 1$, stress response may be stronger than neo-Hookean description by a factor of $Wi_s^{1/4}$. This occurs even at small strains. The second effect is associated with polymer entanglement that VHB exhibits in this study. If entanglement relaxes on the time scale of τ_{ent}, then the entanglement is expected to emerge for $\dot{\varepsilon}\tau_{ent} > 1$, where $\dot{\varepsilon}$ is Hencky rate, boosting intrachain stress. Entanglement emerges at varying levels of strain, depending on sizes of crossing strands that form entanglement. Third, intersegmental interactions can contribute to stress so that tensile stress is no longer entirely intrachain in origin [37]. Such intersegmental stress occurs at lower temperature or much higher rates. These three factors can (1) affect the bond tension buildup and therefore indirectly affect the network lifetime and (2) increase the magnitude of energy release rate at fracture (G_c). However, these viscoelastic effects do not entail any additional timescale. Bond dissociation kinetics is the sole mechanism that defines the internal clock. Specifically, polymer viscoelasticity may affect the timescale on which bond dissociation occurs, but it does not create a separate clock to measure external conditions associated with rate and temperature. Future studies will demonstrate these effects in more detail, especially the interchain effect.

4.2. Internal clock from bond dissociation theory

Recent spatial-temporal resolved polarized optical microscopic (*str*-POM) measurements [26] of the strain field at the crack tips have provided fresh insights into the nature of polymer fracture. These *str* -POM experiments on elastomers [8,20] show that (a) tip stress can be quantitatively measured, (b) fracture occurs when tip stress is comparable to inherent polymer fracture strength $\sigma_{F(inh)}$, leading to the revelation [30] that toughness (Griffith-Irwin's critical energy release rate G_c) is determined by $\sigma_{F(inh)}$ along with a characteristic length related to the stress saturation zone ahead of the crack tip. These recent studies have led to the suggestion of a specific theory of bond dissociation for elastomeric fracture [30]. Guided by this new theoretical framework, the present work aimed to examine how crack growth takes place in three different elastomers. Treating elastomeric rupture as arising from bond dissociation in backbones of network strands, the theory can readily rationalize the observed dependence of v_c on load and temperature. In other words, elastomeric fracture is qualitatively predictable, and bond lifetime is the hidden molecular clock that depends on the degree of network stretching and increases upon lowering temperature. Specifically, higher stretch rate produces higher loading due to emergence of embedded entanglement in VHB, resulting, as shown in Section 2, in higher crack growth rate. VHB also shows faster crack growth at a higher preload level, as shown in Section 2.2. A rise in temperature makes crack propagate faster at a fixed load, as shown in Section 3.1 with 0.3phrSBR. Finally, xPMA examined in Sections 3.2 and 2.2 confirms that crack propagation is faster at either higher stretch rate or larger stepwise stretch ratios.

Our theory expects the crack propagation velocity $v_c(G_c, T)$ to increase with both the applied load at a given temperature and rising temperature for a given load. It recognizes the following expression for bond lifetime

$$t_b(\bar{f}, T) = t_0 e^{\frac{E_a(\bar{f})}{RT}}. \tag{4}$$

When $v_c \sim 1/t_{ntw}$ and $t_{ntw} \sim t_b$, faster crack growth can be understood to arise from shorter t_b. There is either lower activation barrier E_a (in one mole of bonds), where R is the gas constant, involving a higher load or the fracture takes place at higher temperature for a given load. Applying Kauzmann-Eyring [50] theory for covalent bond dissociation, along with the recent density functional theory (DFT) calculations of Beyer [51], Eq. (4) prescribes a well-known quantitative description of bond scission in presence of normalized bond tension $\bar{f} = f/f_{max}$. Using Morse potential to describe the energy potential [52], an analytical form [30,50,53,54] of $E_a(\bar{f})$ can be derived as $E_a(\bar{f})/D_e = \sqrt{1-\bar{f}} + (\bar{f}/2)\ln\left(\frac{1-\sqrt{1-\bar{f}}}{1+\sqrt{1-\bar{f}}}\right)$, which is known since 1940, where D_e is the bond dissociation energy, equal to 370.8 kJ/mol, and $f_{max} = 6.9$ nN for carbon-carbon bonds according to the DFT calculations [51]. Eq. (4)

implies that bond strength is stronger on short timescales. Consequently, elastomeric fracture strength $\sigma_{F(inh)}$ is hardly a constant [30]. Such conclusions can be readily drawn from any modeling that introduces dynamic bond breakage mechanism [55] for network failure.

To illustrate the effects of rate and temperature on both continuous and stepwise stretching of either notch-free or prenotched elastomers, let us consider the simplest model of an ideal chain network in startup continuous stretching. Such a network is homogeneous, free of entanglement, and comprises of strands of equal length. Bond tension f may be regarded as the same as tension in network strands, i.e., directly proportional to nominal stress $\sigma_{engr} = \psi_{\times} f$. Independent of stretch rate, stress-strain curves overlap for different rates up to failure. It then follows that network lifetime t_{ntw} may explicitly depend on bond lifetime t_b. Under this condition, we can take t_{ntw} to monotonically decreases with σ_{engr} or $f = f_{max}\bar{f}$ per Eq. (4). Fig. 6(a) qualitatively sketches t_{ntw} as a function of σ_{engr} for two temperatures, along with the elapsed stretching time t_s that increases with stretch ratio λ or stress σ_{engr}. Rupture or fracture occurs when the experimental timescale t_s grows to become comparable to the network lifetime, i.e., when the two curves cross. Here t_{ntw} decreases with increasing σ_{engr} per Eq. (4) because $f \sim \sigma_{engr}$, and t_s increases with σ_{engr} per $t_s = (\lambda - 1)/\dot{\lambda}$ because of the monotonic relationship between σ_{engr} and λ. The temperature effect on tensile strength occurs because the network has a shorter lifetime at higher temperature $T' > T$ so that t_{ntw} and t_s meet in Fig. 6(a) at a lower value of σ_{engr} or λ at T'.

Fig. 6(b) shows how the rate effect emerges. At a given temperature and with greater rate, e.g.,$\dot{\lambda} > \dot{\lambda}'$, it takes less time to produce the same stress level. Upon reaching the λ value marked by the vertical dashed line (at which the resulting engineering stress is σ_1), less time ($t_1 < t_1$') has elapsed relative to t_1' spent by the slow test (with $\dot{\lambda}$'); the network lifetime at σ_1 is much longer than stretching time t_1. For the network to fail on the timescale of t_1 the network would need to be stretched to a higher stress indicated by σ_2. Thus, the stretching can continue beyond the point where the slow test has produced failure (rupture or fracture), until more bond tension builds up to cause the lifetime to shorten. Clearly, faster stretching results in high tensile strength and toughness, as shown in this study.

Fig. 6(c) shows how the temperature effect on crack growth after stepwise stretching can be anticipated. At any given stress or stretching level, the network lifetime shortens as temperature increases from T_1 to T_3. In terms of the bond dissociation theory for elastomeric rupture [30], we interpret crack propagation velocity v_c to be reciprocally related to t_{nwt}. Thus, v_c is expected to change with temperature as $v_c \sim e^{\frac{-E_a(\bar{f})}{RT}}$ at a fixed value of $\bar{f}$, showing three different values of time labeled in Fig. 6(c). Moreover, because barrier height E_a decreases with increasing $\bar{f}$, v_c may increase exponentially with remote stress or energy release rate, as shown in Fig. 1(c) and Fig. 5(b). Higher G_c produces a lower activation energy E_a and shorter lifetime t_{nwt}, leading to a higher v_c. Temperature influences v_c as well as G_c: At a lower temperature network is longer lived so that more stretching can occur, corresponding to higher G_c before fracture.

In passing, we note that the earliest theoretical description [56] of elastomeric rupture involves the concept of bond scission ran into trouble, leading to the conclusion that bond dissociation could occur upon crosslinking a polymer melt. Bueche [57–59] and Halpin [60,61] recognized that the elastomeric rupture involves chain scission. However, their view was obscured by the overwhelming viscoelastic effects that only take place at sufficiently low temperatures [20]. According to them [59,61], polymer relaxation time would determine load transfer from one broken strand to the next.

It is currently a formidable task for us to quantify how global stretching produces bond tension, leading to rupture in notch-free or fracture in prenotched elastomers, because such a description requires (a) explicit knowledge of the network structure and (b) a molecular theory to characterize the effect of global stretching on tension buildup in individual network strands, and (c) percolation of bond dissociation events across the fracture plane, i.e., the plane indefined by the crack growth direction and the thickness direction (orthogonal to the stretching direction). Qualitatively, we can fully comprehend based on the bond dissociation theory [30] why relationships such as those described in Eq. (1) and Eq. (2) arise in the literature of elastomeric fracture.

4.3. Shift factor γ_T unrelated to viscoelasticity

Time dependence of elastomeric fracture, manifested in rate and temperature effects, points to the existence of an internal timescale. In polymeric networks, since temperature affects chain dynamics, polymer relaxation time naturally presents itself as a candidate. However, we assert that the missing or hidden timescale in elastomeric fracture is the network lifetime t_{ntw}, which depends on the degree of stretching, i.e., on the load G_c as well as temperature. In this new picture, the longer lifetime corresponds to slower crack growth. The lower the temperature, the more stretchable the elastomer is due to its longer lifetime. The faster the stretching, the higher the rupture strain, because only a higher degree of strain can build up more bond tension to shorten the network lifetime. At a given load G_c, because $v_c \sim 1/t_{ntw}$ we have

$$v_c(T) t_{ntw}(T, G_c) = v_c(T_{ref}) t_{nwt}(T_{ref}, G_c) \tag{5}$$

or

$$\frac{v_c(T)}{v_c(T_{ref})} = \frac{1}{\gamma_T} = \frac{t_{ntw}(T_{ref}, G_c))}{t_{ntw}(T, G_c)} = \frac{t_b(T_{ref}, \bar{f})}{t_b(T, \bar{f})}. \tag{6}$$

In other words, choosing a reference temperature T_{ref}, A_T in Eq. (2) is γ_T, not WLF shift factor a_T. Thus, for a common load, measurements of v_c at different temperatures can be used to reveal the temperature dependence of the internal clock. Although a direct relationship between t_{ntw} and t_b is unavailable, as far as the temperature dependence of the shift factor γ_T is concerned, we postulate in Eq. (6) that the ratio of network lifetimes equals the ratio of bond lifetimes. This factor is conceptually different from the WLF shift factor and is only well defined for an elastomer under a common load G_c, which prescribes the same level of bond tension, corresponding to the same activation energy E_a in Eq. (4). Stepwise stretching tests show in Fig. 3(a)-(b) that v_c vary with temperature in an Arrhenius manner instead of following the WLF shift factor.

4.4. Clarification of time dependence

For both prenotched and notch-free specimens, stretch rate conveniently prescribes an external timescale on which fracture or rupture takes place. Specifically, the reciprocal stretch rate is the timescale for continuous stretching of notch-free elastomers. In the case of prenotching specimens, stress buildup occurs on a timescale prescribed by the global stretch rate $\dot{\lambda}$. Higher crack propagation velocity v_c is seen to involve higher load or energy release rate G_c, confirmed by all data presented in Sections 2 to 3. The phenomenology of elastomeric fracture and rupture at different rates and temperatures comprises of two parts. The first part pertains to what sets up the timescale of fracture, e.g., the magnitude of v_c. The second part concerns the origin of a monotonic relationship between v_c and G_c. Here we avoid an additional aspect, extensively reported in the literature [4,9,62,63] that there is a discontinuous transition [47], where v_c is double-valued at a given G_c – the transition was responsible for dashed lines in Fig. 8(a) in Section 4.7.

In the search for the origin of time dependence (i.e., rate or temperature dependence) of elastomeric fracture, the past research of seven decades focused on the second part, i.e., on explaining why G_c increases with v_c, summarized by Eq. (1). It did so by inferring a timescale t_{ve} from v_c by postulating existence of an unknown length scale δ: $t_{ve} = \delta/v_c$.

Specifically, the increase of the second term in Eq. (1) with v_c is interpreted to arise from energy dissipation: Viscoelastic effects are stronger at a higher rate or lower temperature; separately it was asserted [11] that $G_c(v_c/\delta) \sim G'(\omega)$. In making such a correlation [11,49,64,65], δ must be on the order of 1 Å, which is smaller by two orders of magnitude than the smallest length scale in the system, e.g., the network mesh size $l_\times \sim$ ca. 5–10 nm. We agree [20] with the recent analysis [65] that in typical elastomers "linear viscoelastic dissipation is negligible" at high temperatures and cannot produce the phenomenon summarized by Eq. (1). However, such considerations [7,11,14,15,21–24] did not explain why the polymer relaxation time would prescribe the crack propagation velocity v_c. In other words, the relationship between G_c and v_c has remained elusive.

Fracture occurs when enough network stretching has occurred to shorten the network lifetime t_{ntw}. In the absence of a detailed molecular model that is based on network structure, we are unable to quantify a relationship between t_{ntw} and stress state at crack tip. On the other hand, it is sensible to expect v_c to be proportional to $1/t_{ntw}$, which depends on bond tension per $t_{ntw} \sim t_b$ of Eq. (4). Higher v_c arises from a higher tip stress state. Data presented in Sections 2.1 and 3.2 show that at a higher stretch rate crack growth occurs at larger remote load and is therefore faster. As for the second part of the phenomenology, there exists a correlation between v_c and G_c at different stretch rates, as shown in Sections 2.1 and 3.2. The correlation can be more directly examined using stepwise stretch to different stretch ratio, as shown in Sections 2.2 and 3.3. Finally, the temperature dependence of v_c can be unambiguously demonstrated using stepwise stretching at different temperatures as shown in Section 3.1.

4.5. Internal clock and shift function (G_c)

Faster stretching apparently can cause higher tensions in load-bearing network strands at rupture. The kinetics of bond dissociation determines the rate and temperature dependencies. In the case where no flaws are large enough to affect tensile strength σ_b of notch-free specimens, which is the case perhaps except for heavily crosslinked elastomers, the experimental timescale is straightforwardly specified by $\dot{\lambda}$. Smith and coworker reported [45,66–68] a family of curves of σ_b vs. $\dot{\lambda}$ to show that curves collected at lower temperatures resides above those measured at higher temperatures (cf. Fig. 8(b) in Section 4.7). Such results suggest the existence of an internal timescale that is also temperature dependent. What is this internal clock? To account for the temperature effect, it is common to carry out a horizontal shift of original curves along the $\dot{\lambda}$ axis. When the resulting shift factor A_T resembled WLF shift factor a_T, the literature asserted that polymer viscoelasticity was at play and the characteristic polymer relaxation time τ was the internal timescale. The identification of A_T as a_T implies that tensile strength σ_b is a monotonic increasing function of Weissenberg number $Wi = \dot{\lambda}\tau$. However, there is no theoretical argument or explanation for why Wi is a controlling parameter, i.e., why σ_b would increase either when τ increases upon lowering temperature or when stretching is faster ($\dot{\lambda}$ is larger) at a given temperature in purely elastic stretching, evidenced by rate-independent stress vs. curves.

An alternative rationale for the temperature effect recognizes that the network lifetime t_{ntw} explicitly depends on temperature like t_b of Eq. (4) does. The observed temperature dependence, e.g., shown in Fig. 3 (a)-(b), reveals that t_{ntw} is the hidden internal timescale. In the elastic stretching limit [30] the elapsed time $t_{rupture}$ at rupture reflects network lifetime, i.e., t_{ntw} and $t_{rupture}$ are proportional to each other at different stretch rates. Thus, the increase of σ_b with rupture strain $\dot{\lambda}t_{rupture}$ reveals that σ_b is an increasing function of $\dot{\lambda}t_{ntw}$. Analogous to Weissenberg number Wi introduced to measure the degree of maximum elastic deformation within the relaxation time τ and to reveal scaling of yield stress in startup shear [69] with Wi, here we introduce a new parameter and call it

$$Wg = \dot{\lambda}t_{ntw}(T), \tag{7}$$

to quantify the degree of attainable stretching before fracture or rupture within the network lifetime t_{ntw}. In other words, like the analogy γ_T of Eq. (6) to a_T, Wg is analogous to Wi, except that Wi varies only with temperature but Wg is a complicated function of the state of stretching and temperature. When Hencky rate $\dot{\varepsilon}$ is applied, $\dot{\lambda}$ in Eq. (7) is replaced by $\dot{\varepsilon}$. Clearly, Wg increases (a) with applied rate and (b) upon lowering temperature that increases the network's lifetime t_{ntw}. In general, σ_b is an increasing function of Wg. In other words, the temperature dependence of σ_b stems from that of Wg.

4.6. Rising tensile strength with stretch rate and lowering temperature

In the topic of time-dependent elastomeric fracture, treated in the energy-based framework of Griffith and Irwin, it is rare to bring about any discussion of rupture characteristics of notch-free specimens, e.g., higher tensile strength and specimens being more stretchable at larger stretch rates and lower temperatures. The prevailing paradigm may not regard this phenomenon as surprising for two reasons. First, continuous stretching until rupture of notch-free elastomers has often been regarded as fracture-mechanical phenomenon based on the assumption that there are large flaws to cause the observed tensile strength to be much lower than inherent strength. Thus, the rate or temperature dependence of the nominal strength was usually thougth to arise from the same dependencies of toughness. Unfortunately, when L_{fc} is large, e.g., ca. 0.1~1 mm, as is the case for lightly to moderately crosslinked rubbery polymers and certainly for VHB in this study, there are no flaws of such a large size. The *str*-POM observations of a sizable stress saturation zone at the crack tip support the general idea that the stretching of notch-free elastomers to rupture measures inherent strength [8,20]. Clearly, there have not been any convincing viscoelastic argument to explain why tensile strength should increase with stretch rate in the limit of purely elastic stretching [48]. In other words, unlike toughness that invokes rate-dependent energy dissipation, it seemed more difficult to explain why tensile strength rises upon lowering the experimental temperature or increasing the stretch rate in the purely elastic stretching limit where Bueche-Halpin theory [60] is clearly inapplicable [20].

Second, to explain rate and temperature effects on rupture characteristics, a notch-free elastomer was perceived [68] to form microcracks that eventually grow unstable. This instability was assumed to resemble Irwin-Griffith fracture, which could be characterized in terms of energy release rate, as explicitly stated by Smith. However, such an account failed to emphasize the condition for initial microcrack formation. Unlike crazing that has often been regarded a precursor to brittle fracture in glassy polymers [70], there is no evidence that emergence of "microcracks" and rupture did not take place nearly at the same moment in continuous stretching, involving the same load level. Nevertheless, influenced by Bueche [57] and Halpin [61], Smith [68] asserted "because the rate of crack growth…, is controlled by the viscous characteristics of an elastomer, the tensile strength σ_b… depend strongly on the temperature and extension rate." In elastomers where the tensile strength is not expected to have suffered a significant reduction due to flaws, Rankine's maximum principal stress theory suggests that the dependence of tensile strength on rate and temperature implies that the inherent strength varies on different timescales, e.g., higher on short timescales.

Tensile strength σ_b of elastomers is known in the literature to increase with increasing stretch rate and decreasing temperature, as reviewed below in Section 4.7. An ideal, uniform structure, corresponding to network strands of the same length, may be expected to show reduced rate dependence: No rupture could occur, and bond tension would not be high enough to produce dissociation until a common stretch ratio is reached. Such rate insensitivity in an ideal network arises because network lifetime is a sharp function of bond tension. A

vulcanized rubber usually is a heterogeneous network and shows significant dependence of ultimate stress and strain on temperature and stretch rate. Until experimental tools become available to characterize the structure of an elastomer, we cannot predict its strength, let alone its dependence on rate and temperature.

For example, Fig. 7(a) shows the temperature effect at a given stretch rate. The same SBR described in Fig. 3(a)-(b) shows remarkable improvement in stretchability and tensile strength over a temperature range of 70 °C. It ruptures at nearly double the initial length at −10 °C but extends only 20 % at 60 °C. At 90 °C, VHB shows a trend in Fig. S2 in SM, showing that VHB is more stretchable at a higher rate. Both figures are consistent with Smith's report shown in Fig. 8(b) in Section 4.7. Past studies have not been able to explain this temperature effect without invoking temperature dependence of polymer dynamics or viscoelasticity. On the other hand, the overlap of symbols in Fig. 7(a) and Fig. S2 shows that chain dynamics at the strand level are still too fast to lead to any viscoelasticity.

The phenomenon shown in Fig. 7(a) cannot be explained in terms of polymer dynamics. For example, given the temperature dependence of the WLF shift factor a_T, we can stretch the SBR using the same effective stretch rate $\dot{\lambda}a_T$ at different temperatures. At a common effect rate of 0.43 min^{-1}, Fig. 7(b) shows, based on a different batch of 0.3phrSBR, that it did not undergo rupture at the same stretch ratio and displayed instead different levels of tensile strength, i.e., higher at lower temperature. This result contradicts the notion that tensile strength should be a function of *Wi*. In our theory, rupture strain approximately increases with *Wg* of Eq. (7), due to increase of t_{ntw} with decreasing temperature. Higher rupture strain and corresponding higher tensile strength occur at lower temperature at a common effective rate crudely imply that the temperature dependence of *Wg* is stronger than that prescribed by the WLF factor a_T. In other words, the data in Fig. 7(b) can be anticipated from the inset figure in Fig. 3(b). Namely, network lifetime t_{ntw} in Eq. (7) increases more strongly than τ does upon temperature decrease. Consequently, when the applied rate is reduced at a lower temperature according to a_T, the SBR is still stronger. Since the temperature dependence of t_{ntw} depends on the barrier height, the trend may change when step stretch tests involve a different level of stretching or when the chosen effective Weissenberg number is different.

4.7. Connection between toughness and tensile strength

In the literature tensile strength [66] and toughness [4] of vulcanized rubbers have often been separately investigated as a function of stretch rate at different temperatures. For example, Greensmith and Thomas showed [4] in Fig. 8(a) that toughness or tearing energy T_c increases with stretch rate and is higher at lower temperature. Separately, Smith showed [66] in Fig. 8(b) that tensile strength σ_b increases with stretch rate and is higher at a lower temperature.

On the one hand, horizontal WLF like shifts were independently made to construct master curves for both T_c and σ_b. On the other hand, no connection has been generally made between the two quantities until a recent series of investigations [20,26,30,48] that explored the hidden connection between these two material quantities through Inglis-like relationship.

Upon a closer examination, Fig. 8(a′) reveals that no shifts can achieve a smooth superposition, contrary to Mullins' claim of a master curve [13] that omitted the data containing dashed lines in Fig. 8(a). Mullins emphasized [13] in Fig. 4 of his paper that the shift factor was different from the WLF shift factor. Nevertheless, he still suggested that the shift represents temperature dependence of viscosity, without acknowledging that the WLF shift is nothing else but a reflection of temperature dependence of viscosity. Another study also reported [71] that the WLF factor from linear viscoelastic data could not shift the fracture toughness of a model polyurethane under purely elastic stretching to achieve a master curve. Today we understand why the two shift factors in the inset of Fig. 3(b) are found to be different. Thus, no smooth master curve should be expected because, unlike the polymer relaxation time, the internal timescale, i.e., the network lifetime depends on both temperature and the degree of stretching [30]. In other words, *Wg* is a more complicated parameter, different from *Wi*.

Similarly, when Smith's data are horizontally shifted to the left relative to the data collected at $T_{ref} = -48.4$ °C, we do not obtain a master curve, as shown in Fig. 8(b′), which contradicts Kinloch's reproduction of the same data. It is plausible that Kinloch constructed the "master curve" in his book [45] without following the WLF shift factor supplied by Smith [66] in the original paper. The difficulty facing the past description of elastomeric fracture is not a quantitative one because the difference between conventional viscoelastic models and bond dissociation theory for elastomeric fracture is qualitative.

The bond dissociation theory for elastomeric rupture offers a realistic explanation of rate and temperature dependencies of tensile strength and toughness [30]. An notch-free elastomer may stretch more before rupture at either higher rate or lower temperature because the network lifetime changes relative to the experimental timescale set by stretch rate, corresponding to a larger value of *Wg*. In other words, when either $\dot{\lambda}$ (or $\dot{\varepsilon}$) is higher or t_{ntw} is larger (at lower temperature), elastomers can be stretched to higher stretch ratio and correspondingly higher strength before rupture. Since toughness is proportional to tensile strength, rate and temperature effects on toughness are similar.

4.8. Issue with timescale shift

Finally, we comment on the nature of shifting tearing (or peeling) energy T_c ($\sim G_c$) vs tearing speed v_c curves at different temperatures, a practice that started in the early stage [7] of research on rubber fracture, as shown in Fig. 8(a′). Similarly, ever since the beginning [66], the same exercise was carried out for tensile strength vs. stretch rate at different temperatures, as shown in Fig. 8(b′). For both tearing energy T_c and tensile strength σ_b, lower temperature produces higher values. It is tempting to build master curves by making horizontal shifts without comprehending the meaning of such a construction. In contrast, we fully understand why the WLF shift [16] collapses small-amplitude oscillatory shear (SAOS) measurements of storage and loss moduli G′(ω, T) and G"(ω, T) of polymeric liquids well above the glass transition temperature: G′ and G" form master curves when plotted against ωa_T because they are only function of $\omega\tau$, where $\tau(T)$ is the relaxation time and $a_T = \tau(T)/\tau(T_{ref})$. For viscoelastic polymeric liquids, τ is the internal clock against which the external timescale (e.g., ω) is measured, as straightforwardly demonstrated by the Maxwell model, according to which G′ and G" only depend on Deborah number $\omega\tau$. In other words, in polymer rheology, the WLF shift to produce master curves for G′ and G" merely confirms that temperature dependence of viscoelasticity arises from that of τ.

Mathematically, taking the lowest curve as reference, any family of curves of increasing function y(x) like those in Fig. 8(a)-(b) can be forced to undergo a horizontal shift to the right. The question is what such a shift implies. The discovery of WLF shift in linear viscoelastic measurements of polymeric liquids [16] perhaps inspired Greensmith *et al.* [13] and Smith [66] to carry out horizontal shifts of tearing energy $G_c(v_c,T)$ and tensile strength $\sigma_b(\dot{\lambda},T)$ along the v_c axis or stretch rate $\dot{\lambda}$ axis (in contrast to the oscillation frequency ω). The shift factor for either G_c or σ_b must be a time ratio. Since the WLF shift factor is a time ratio, it is not surprising for past studies to adopt the WLF factor a_T. The question is whether Fig. 8(a′) and (b′) hint at something entirely different.

The origin of the stacking shown in Fig. 8(a′) and 8(b′) is temperature dependence of lifetime t_{ntw}. Consequently, master curves obtained from horizontal shifts can be only approximate, as shown in Fig. 8(a′), which happens because temperature dependence of v_c is different at different loading levels, represented by G_c. The lack of the superposition is rather evident in the literature but often overlooked [9]. The superposition fails

because the data do not involve a fixed value of G_c.- *Wg* is a well-defined function of temperature only when the degree of network stretching is fixed. When a single value of G_c operates, Eq. (6) may describe the data in Fig. 3(b): Instead of τ, the network lifetime t_{ntw} is the controlling timescale.

In summary, the shifts of data such as those of G_c and σ_b in Fig. 8(a)-(b) are highly complex because it involves data acquired at different levels of G_c that prescribe different temperature dependencies of network lifetime per Eq. (4). In Eq. (4), t_b depends on G_c because the activation energy E_a, given in terms of the bond tension $\bar{f}$, changes with G_c. Simply put, the internal clock (network's lifetime) for elastomeric fracture varies with both temperature and loading.

4.9. A further comment on "energy dissipation"

For elastomers, it has been elusive why G_c is so much greater than surface energy Γ. It is thus common in fracture mechanics literature including the literature on elastomeric fracture, to see the phrase *energy dissipation* in discussions of toughness G_c. Moreover, the positive correlation between G_c and v_c further encouraged researchers to explain the origin of the phenomenology summarized by Eq. (1) – Mullins and others [7,9,13] literally took "energy dissipation" to mean that elastomeric fracture involves viscous dissipation. Reduced toughness of solvent-swollen elastomers has been correlated with a decrease of loss modulus [9,38,39].

The essence of the Lake-Thomas model [25] is to argue that G_c represents elastic energy release instead of the energy "dissipation" associated with bond dissociation. However, its estimate could not deal with the rate and temperature effects because it did not describe how bond strength varies with time and temperature. Consequently, it cannot be regarded as a successful theory for elastomeric fracture. In absence of a detailed structural model to account for some unknown process taking place at crack tip, *energy dissipation* is conveniently invoked to describe what happens in the so-called process or fracture zone and around crack tip (in the so called bulk) [15,44,72]. While bond dissociation releases the stored bond energy (as perceived by Lake-Thomas) which is not straightforward to recollect, such energy has nothing to do with dissipation that is commonly associated with viscous stress, which Mullins [13] used to account for the rate dependence of toughness. Instead of a monolayer of chains in a highly stretched state, as described by the Lake-Thomas model, there seem to be two layers of thickness much greater than molecular scales on either side of the fracture surface where chains may be highly stretched in their elastic state. The high magnitude of G_c stems from the fact that there exists such a sizable region of high stress, which amounts to a high level of energy storage at crack tip, to be released upon crack growth [8,26,30].

In explaining rate and temperature dependencies of G_c, we point out that the energy release upon fracture is *not* synonymous with *energy dissipation* that should only be used to refer to viscous dissipation. Unfortunately, the association of toughness with energy dissipation is widespread in the literature [44,73,74]. It is customary for researchers to associate the existence of a sizable Mullins hysteresis loop [75–78] with high energy dissipation. In the case of unfilled elastomers that contain a significant amount of trapped entanglement, the meaning of sizable hysteresis loop requires clarification. Uncrossability, giving rise to what we call entanglement, acts like chemical crosslinks during fast "forward" stretching. During retraction in a hysteresis test, such transient junctions tend to vanish because the stretching-induced uncrossability constraint is released causing the "backward" stress to lose the entanglement contribution. The existence of appreciable hysteresis loop cannot be used as evidence to suggest that the forward stretching involves any dissipative process. In other words, it is problematic to correlate high toughness with large "energy dissipation" and existence of a large hysteresis loop. There are no shortage of cases showing high toughness with little evidence of energy dissipation, i.e., negligible hysteresis loop size [73,74,79]. In fact, a phase "elastic dissipator" was invented [80] to preserve the conventional depiction of fracture toughness in terms of energy dissipation, where the principal reason to invoke this concept was the desire to explain $G_c >> \Gamma$.

5. Conclusion

The phenomenology given Eq. (1) has been widely reported and known since the pioneering studies of Thomas and coworkers [3,4], tensile strength is similarly rate and temperature dependent, as shown by Smith and coworkers [66,67]. The past theoretical explanations [7,11,14,15,21–24] have been based on the introduction of polymer relaxation time as the internal clock. Thus, elastomeric fracture has been known as a type of viscoelastic fracture [64,65]. These treatments were conveniently made within the conventional paradigm of fracture mechanics that describes fracture in terms of the energy release rate. In the stress-based approach [30] based on a familiar fracture mechanism [81,82], material strength dictates fracture. There is no concern or confusion about why toughness is much higher than surface energy. This alternative paradigm readily leads us to the identification of the hidden internal clock responsible for the observed rate and temperature dependencies.

Experiments and theoretical analyses reported in this study have allowed us to make the following conclusions. In short, network stretching causes high bond tension to emerge that prescribes the timescale for bond dissociation and network rupture. While the current study presented a conceptual picture of elastomeric fracture and clarified the causal relationship, a molecular level structural model has yet to be developed for quantitative description. In short, we can make the following summary.

<u>On the experimental side</u>

1. Pure shear at different stretch rates allows crack propagation to occur at loads (i.e., different values of toughness G_c) involving different speed v_c.
2. Crack growth is faster at higher temperatures.
3. Faster stretching produces higher tensile strength and higher toughness either in presence or in absence of entanglement (viscoelastic effect).
4. Rate and temperature effects on G_c and v_c take place in absence of polymer viscoelasticity.

<u>On the theoretical or foundational side</u>

5. The origin of $G_c >> \Gamma$ is emergence of an extensive region of high elastic stress around the crack tip according to *str*-POM observations – the corresponding elastic energy would be released during crack growth. It is thus confusing and misleading to equate toughness with energy dissipation, as stated [83] "the value (of G_c) was about 10 kJ/m^2-some orders of magnitude greater than any true surface energies-confirming that irreversible processes dominate tear behavior" and "these observations [13] established that internal viscosity is a dominant factor in determining the tear strength of such materials". This is simply incorrect.
6. Crack growth rate depends on the degree of network stretching from which G_c can be evaluated. To reiterate, stretching (corresponding G_c) is the cause, and crack speed v_c is the effect.
7. The elastomer's network lifetime is the internal clock and is the origin of rate and temperature dependencies in rupture and fracture.
8. Rate and temperature dependencies of toughness and tensile strength should not be described using the WLF shift factor; rate-dependent stress response may stem from participation of entanglement in load bearing. Such viscoelastic behavior has

little to do with viscous dissipation related to viscous component of stress.

9. Toughness G_c indicates the load level, which determines network lifetime. Consequently, higher strain in prenotched system results in faster crack propagation speed v_c. G_c is the cause not the effect. Our new description is to replace Eq. (1) with Eq. (2), i.e., to recognize the imposed strain as the cause of fracture and crack propagation. At lower temperatures where there is less thermal energy to drive bond dissociation, only higher G_c can produce the same v_c observed at higher temperature with lower G_c. In other words, the temperature effect on G_c stems from temperature's influence on network lifetime.
10. Viscoelastic effects including entanglement, intermolecular contributions to stress at temperatures close to the glass transition temperature may affect the bond tension buildup to indirectly influence the magnitude of tensile strength and toughness. Additional research remains to be performed in the future.
11. It is always the bond dissociation that prescribes the timescale for crack growth. Higher crack propagation speed v_c involves shorter lifetime (t_{ntw}) in presence of higher network stretching and correspondly higher energy release rate G_c.

6. Materials and methods

6.1. Materials and sample preparation

Samples under study are commercial VHB4910 (3 M product), crosslinked SBR acquired from Goodyear (SLF® 16S42). To guarantee transparency, crosslinking agent dicumyl peroxide (DCP) for SBR is the only additive. The amount of DCP (Acros Organics) is 0.3phr so the samples are labeled as 0.3SBR respectively. SBR sheets with thickness 1.5 mm were cured by heat compression molding at 160 °C for 60 minutes.

Crosslinked poly(methyl acrylate) (xPMA) are made as follows. The crosslinker butanediol diacrylate (208 μL, 1.1 mmol, 1 equiv) and the photoinitiator Irgacure 819 (46.2 mg, 0.11 mmol, 0.1 equiv) were dissolved in a 1:1 (v/v) mixture of methyl acrylate (MA) (10 mL, 110 mmol, 100 equiv) and chloroform (10 mL). The solution was then thoroughly deoxygenated by 20 min of nitrogen purging before being transferred via a syringe under nitrogen protection to a Glass-Silicone-Glass sandwich mold (120 mm × 120 mm × 1.4 mm). After UV irradiation (wavelength = 365 nm) for 1 h, the cured film was taken out from the mold and submerged in toluene to remove any sol fraction. The solvent was decanted and replaced with fresh one three times over the course of 24 h. The washed film was then deswollen in methanol and dried under air for 1 h and then on high vacuum at 50 °C for 24 h. Different batches can differ slightly in the glass transition temperature T_g, due to variation of network defects associated with the number of dangling chains, topological loops etc.

Type V die (ASTM D638) was used to make uncut specimens of dogbone shape (width of ca. 3.2 mm and gauge length of 9.5 mm). Local stretch ratio is measured by video recording of distance between two marks painted in the gauge section as a function of time or nominal stretch ratio, allowing true stress to be quantified along with *in situ* birefringence measurements. The established stress-optical relationship (SOR) is used to determine the stress field at notch tip. Ribbon like specimens with two different dimensions were cut by a paper cutter. Single-edge notch (SEN) and pure shear test pieces are made by gently pushing a razor blade (Feather Safety Razor Co., Ltd.) into the specimens. For SEN samples the length by width dimension is 30 × 15 mm^2, and the cut size to width ratio (a/W) is kept as 0.2. For pure shear, the test pieces between clamps are measured to have dimensions with width ranging from 60 to 100 mm and cut length between 24 and 30 mm, and height of 10 mm.

6.2. Methods

Tensile experiments at various temperatures were carried out using an Instron 5567 tensile tester equipped with 100 N load cell (2525–807), with environmental chamber. Birefringence setup is standard and has been previously described [8,20,26].

CRediT authorship contribution statement

Zehao Fan: Visualization, Formal analysis, Data curation. **Shi-Qing Wang:** Writing – review & editing, Writing – original draft, Validation, Supervision, Project administration, Methodology, Investigation, Funding acquisition, Formal analysis, Conceptualization. **Ming-chi Wang:** Formal analysis, Data curation. **Asal Siavoshani:** Visualization, Formal analysis, Data curation. **Junpeng Wang:** Supervision.

Declaration of Competing Interest

The authors declare that they have no known competing financial interests or personal relationships that could have appeared to influence the work reported in this paper.

Acknowledgments

This work is supported, in part, by the Polymers program at the US National Science Foundation (DMR-2210184). JW acknowledges support from the US National Science Foundation (CHE 2204079). SQW appreciates numerous communications by email with Rong Long and Rui Huang.

Appendix A. Supporting information

Supplementary data associated with this article can be found in the online version at doi:10.1016/j.eml.2024.102277.

Data availability

Data will be made available on request.

References

[1] A.A.V.I. Griffith, The phenomena of rupture and flow in solids, Philos. Trans. R. Soc. Lond. Ser. A, Contain. Pap. A Math. Or. Phys. Character 221 (582-593) (1921) 163–198.
[2] Irwin, G.R. In Onset of fast crack propagation in high strength steel and aluminum alloys, 1956; Sagamore Research Conference Proceedings: 1956; pp 289-305.
[3] R. Rivlin, A.G. Thomas, Rupture of rubber. I. Characteristic energy for tearing, J. Polym. Sci. 10 (3) (1953) 291–318.
[4] H.W. Greensmith, A. Thomas, Rupture of rubber. III. Determination of tear properties, J. Polym. Sci. 18 (88) (1955) 189–200.
[5] R. Long, C.-Y. Hui, Crack tip fields in soft elastic solids subjected to large quasi-static deformation—a review, Extrem. Mech. Lett. 4 (2015) 131–155.
[6] C. Chen, Z. Wang, Z. Suo, Flaw sensitivity of highly stretchable materials, Extrem. Mech. Lett. 10 (2017) 50–57.
[7] H. Greensmith, L. Mullins, A. Thomas, Rupture of rubber, Trans. Soc. Rheol. 4 (1) (1960) 179–189.
[8] Z. Fan, S.-Q. Wang, Resolving stress state at crack tip to elucidate nature of elastomeric fracture, Extrem. Mech. Lett. 61 (2023) 101986.
[9] K. Tsunoda, J. Busfield, C. Davies, A. Thomas, Effect of materials variables on the tear behaviour of a non-crystallising elastomer, J. Mater. Sci. 35 (20) (2000) 5187–5198.
[10] G.R. Irwin, Analysis of stresses and strains near the end of a crack transversing a plate, Trans. ASME, Ser. E, J. Appl. Mech. 24 (1957) 361–364.
[11] A. Gent, Adhesion and strength of viscoelastic solids. Is there a relationship between adhesion and bulk properties? Langmuir 12 (19) (1996) 4492–4496.
[12] H. Greensmith, Rupture of rubber. VIII. Comparisons of tear and tensile rupture measurements, J. Appl. Polym. Sci. 3 (8) (1960) 183–193.
[13] L. Mullins, Rupture of rubber. IX. Role of hysteresis in the tearing of rubber, Trans. Inst. Rubber Ind. 35 (5) (1959) 213–222.
[14] B. Persson, E. Brener, Crack propagation in viscoelastic solids, Phys. Rev. E 71 (3) (2005) 036123.
[15] C. Creton, 50th anniversary perspective: Networks and gels: Soft but dynamic and tough, Macromolecules 50 (21) (2017) 8297–8316.

[16] M.L. Williams, R.F. Landel, J.D. Ferry, The Temperature Dependence of Relaxation Mechanisms in Amorphous Polymers and Other Glass-forming Liquids, J. Am. Chem. Soc. 77 (14) (1955) 3701–3707.
[17] A. Gent, J. Schultz, Effect of wetting liquids on the strength of adhesion of viscoelastic material, J. Adhes. 3 (4) (1972) 281–294.
[18] E. Andrews, A. Kinloch, Mechanics of elastomeric adhesion, in: Journal of polymer science: polymer symposia, 1974, Wiley Online Library, 1974, pp. 1–14.
[19] D. Maugis, M. Barquins, Fracture mechanics and the adherence of viscoelastic bodies, J. Phys. D: Appl. Phys. 11 (14) (1989) 1978.
[20] S.-Q. Wang, Z. Fan, Investigating the dependence of elastomeric fracture on temperature and rate, Rubber Chem. Technol. 96 (4) (2023) 530–550.
[21] P. De Gennes, Weak adhesive junctions, J. De. Phys. 50 (18) (1989) 2551–2562.
[22] J.M. Bowen, W.G. Knauss, The characterization of the energy of fracture at or near interfaces between viscoelastic solids, J. Adhes. 39 (1) (1992) 43–59.
[23] P.-G. de Gennes, Soft adhesives, Langmuir 12 (19) (1996) 4497–4500.
[24] W.G. Knauss, A review of fracture in viscoelastic materials, Int J. Fract. 196 (1-2) (2015) 99–146.
[25] G. Lake, A. Thomas, The strength of highly elastic materials, Proc. R. Soc. Lond. A 300 (1460) (1967) 108–119.
[26] T. Smith, C. Gupta, Z. Fan, G.J. Brust, R. Vogelsong, C. Carr, S.-Q. Wang, Toughness arising from inherent strength of polymers, Extrem. Mech. Lett. 56 (2022) 101819.
[27] B. Deng, S. Wang, C. Hartquist, X. Zhao, Nonlocal intrinsic fracture energy of polymerlike networks, Phys. Rev. Lett. 131 (22) (2023) 228102.
[28] M.K. Chaudhury, Rate-dependent fracture at adhesive interface, J. Phys. Chem. B 103 (31) (1999) 6562–6566.
[29] A. Ghatak, K. Vorvolakos, H. She, D.L. Malotky, M.K. Chaudhury, Interfacial rate processes in adhesion and friction, J. Phys. Chem. B 104 (17) (2000) 4018–4030.
[30] S.-Q. Wang, Z. Fan, C. Gupta, A. Siavoshani, T. Smith, Fracture behavior of polymers in plastic and elastomeric states, Macromolecules 57 (9) (2024) 3875–3900.
[31] S.R. Lavoie, R. Long, T. Tang, A rate-dependent damage model for elastomers at large strain, Extrem. Mech. Lett. 8 (2016) 114–124.
[32] H.M. van der Kooij, S. Dussi, G.T. van de Kerkhof, R.A. Frijns, J. van der Gucht, J. Sprakel, Laser Speckle Strain Imaging reveals the origin of delayed fracture in a soft solid, Sci. Adv. 4 (5) (2018) eaar1926.
[33] J. Wang, B. Zhu, C.-Y. Hui, A.T. Zehnder, Delayed fracture caused by time-dependent damage in PDMS, J. Mech. Phys. Solids 181 (2023) 105459.
[34] J. Ju, G.E. Sanoja, M.Y. Nagazi, L. Cipelletti, Z. Liu, C.Y. Hui, M. Ciccotti, T. Narita, C. Creton, Real-time early detection of crack propagation precursors in delayed fracture of soft elastomers, Phys. Rev. X 13 (2) (2023) 021030.
[35] M. Pharr, J.-Y. Sun, Z. Suo, Rupture of a highly stretchable acrylic dielectric elastomer, J. Appl. Phys. 111 (10) (2012).
[36] D.F. James, Boger fluids, Annu. Rev. Flu. Mech. 41 (1) (2009) 129–142.
[37] H. Sun, G. Liu, K. Ntetsikas, A. Avgeropoulos, S.-Q. Wang, Rheology of entangled polymers not far above glass transition temperature: transient elasticity and intersegmental viscous stress, Macromolecules 47 (16) (2014) 5839–5850.
[38] K. Cho, W.J. Jang, D. Lee, H. Chun, Y.-W. Chang, Fatigue crack growth of elastomers in the swollen state, Polymer 41 (1) (2000) 179–183.
[39] H. Wang, K. Wang, W. Fan, S. Cai, Rupture of swollen styrene butadiene rubber, Polym. Test. 61 (2017) 100–105.
[40] D.J. Plazek, G.F. Gu, R.G. Stacew, L.J. Su, E.D. Von Meerwall, F.N. Kelley, Viscoelastic dissipation and the tear energy of urethane-cross-linked polybutadiene elastomers, J. Mater. Sci. 23 (4) (1988) 1289–1300.
[41] A.N. Gent, Viscoelastic effects in cutting and tearing rubber, Rubber Chem. Technol. 67 (4) (1994) 610–618.
[42] T. Baumberger, C. Caroli, D. Martina, Fracture of a biopolymer gel as a viscoplastic disentanglement process, Eur. Phys. J. E 21 (1) (2006) 81–89.
[43] J. Slootman, V. Waltz, C.J. Yeh, C. Baumann, R. Göstl, J. Comtet, C. Creton, Quantifying rate-and temperature-dependent molecular damage in elastomer fracture, Phys. Rev. X 10 (4) (2020) 041045.
[44] R. Long, C.-Y. Hui, J.P. Gong, E. Bouchbinder, The fracture of highly deformable soft materials: A tale of two length scales, Annu. Rev. Condens. Matter Phys. 12 (2021) 71–94.
[45] A.J. Kinloch, R.J. Young, Fracture Behaviour of Polymers, Springer Science & Business Media, 2013.
[46] I.M. Ward, J. Sweeney, Mechanical Properties of Solid Polymers, 3rd, John Wiley & Sons, Ltd, Chichester, UK, 2012.
[47] Z. Fan, S.-Q. Wang, Discontinuous dynamic transition in crack propagation of stretchable elastomers, Phys. Rev. E 110 (2024) 065001 (to be published.).
[48] Z. Asal Siavoshani, Muxuan Yang, Shan Liu, Ming-Chi Wang, Jiabin Liu, Weinan Xu, Junpeng Wang, Shaoting Lin, Shi-Qing Wang, How rate, temperature and solvent exchange affect polymer network rupture? Soft Matter 20 (2024) 7657–7667. Viscosity of glycerol is higher than that of water by a factor of a thousand. Moreover, for different applied rates, Fig. 2(a) presents the same stress vs. strain curves, and Fig. 2(b) shows that the network underwent the same degree of molecular stretching, indicated by the same level of birefringence, confirming that the elastomeric stretching is purely elastic when the 3M elastomer is stretched at the elevated temperature where entanglement effect vanishes.
[49] W.G. Knauss, On the steady propagation of a crack in a viscoelastic sheet: Experiments and analysis. Deformation and Fracture of High Polymers, Springer, 1973, pp. 501–541.
[50] W. Kauzmann, H. Eyring, The viscous flow of large molecules, J. Am. Chem. Soc. 62 (11) (1940) 3113–3125.
[51] M.K. Beyer, The mechanical strength of a covalent bond calculated by density functional theory, J. Chem. Phys. 112 (17) (2000) 7307–7312.
[52] P.M. Morse, Diatomic molecules according to the wave mechanics. II. Vibrational levels, Phys. Rev. 34 (1) (1929) 57.
[53] B. Crist Jr, J. Oddershede, J. Sabin, J. Perram, M.A. Ratner, Polymer fracture—a simple model for chain scission. J. Polym. Sci., Polym. Phys. Ed. 22 (5) (1984) 881–897.
[54] R. Puthur, K. Sebastian, Theory of polymer breaking under tension, Phys. Rev. B 66 (2) (2002) 024304.
[55] A. Ghareeb, A. Elbanna, Modeling fracture in rate-dependent polymer networks: A quasicontinuum approach, J. Appl. Mech. 88 (11) (2021) 111007.
[56] A. Bueche, The ultimate properties of simple elastomers, J. Polym. Sci. 19 (92) (1956) 275–284.
[57] F. Bueche, Tensile strength of plastics above the glass temperature, J. Appl. Phys. 26 (9) (1957) 1133–1140.
[58] F. Bueche, The tensile strength of elastomers according to current theories, Rubber Chem. Technol. 32 (5) (1959) 1269–1285.
[59] F. Bueche, Tensile strength of plastics above the glass temperature, J. Appl. Phys. 26 (9) (1955) 1133–1140.
[60] F. Bueche, J. Halpin, Molecular theory for the tensile strength of gum elastomers, J. Appl. Phys. 35 (1) (1964) 36–41.
[61] J. Halpin, Fracture of amorphous polymeric solids: time to break, J. Appl. Phys. 35 (11) (1964) 3133–3141.
[62] Y. Morishita, K. Tsunoda, K. Urayama, Velocity transition in the crack growth dynamics of filled elastomers: Contributions of nonlinear viscoelasticity, Phys. Rev. E 93 (4) (2016) 043001.
[63] T.-T. Mai, K. Okuno, K. Tsunoda, K. Urayama, Crack-tip strain field in supershear crack of elastomers, ACS Macro Lett. 9 (5) (2020) 762–768.
[64] C.-Y. Hui, B. Zhu, R. Long, Steady state crack growth in viscoelastic solids: A comparative study, J. Mech. Phys. Solids 159 (2022) 104748.
[65] E. Barthel, The linear viscoelastic fracture theory applies to soft solids better when they are… viscoelastic, Proc. R. Soc. A 480 (2288) (2024) 20230561.
[66] T.L. Smith, Dependence of the ultimate properties of a GR-S rubber on strain rate and temperature, J. Polm. Sci. 32 (124) (1958) 99–113.
[67] T.L. Smith, P.J. Stedry, Time and temperature dependence of the ultimate properties of an SBR rubber at constant elongations, J. Appl. Phys. 31 (11) (1960) 1892–1898.
[68] T.L. Smith, Strength of elastomers. A perspective, Rubber Chem. Technol. 51 (2) (1978) 225–252.
[69] S.-Q. Wang, Nonlinear Polymer Rheology: Macroscopic Phenomenology and Molecular Foundation, Wiley, Hoboken, NJ, 2018.
[70] M. Razavi, S. Cheng, D. Huang, S. Zhang, S.-Q. Wang, Crazing and yielding in glassy polymers of high molecular weight, Polymer 197 (2020) 122445.
[71] A. Cristiano, A. Marcellan, B.J. Keestra, P. Steeman, C. Creton, Fracture of model polyurethane elastomeric networks, J. Polym. Sci. Part B: Polym. Phys. 49 (5) (2011) 355–367.
[72] C. Creton, M. Ciccotti, Fracture and adhesion of soft materials: a review, Rep. Prog. Phys. 79 (4) (2016) 046601.
[73] T. Zhang, S. Lin, H. Yuk, X. Zhao, Predicting fracture energies and crack-tip fields of soft tough materials, Extrem. Mech. Lett. 4 (2015) 1–8.
[74] S.T. Lin, C.D. Londono, D.C. Zheng, X.H. Zhao, An extreme toughening mechanism for soft materials, Soft Matter 18 (31) (2022) 5742–5749.
[75] J.A.C. Harwood, L. Mullins, A.R. Payne, Stress softening in natural rubber vulcanizates. Part II. Stress softening effects in pure gum and filler loaded rubbers, J. Appl. Polym. Sci. 9 (9) (1965) 3011–3021.
[76] J.A.C. Harwood, A.R. Payne, Stress softening in natural rubber vulcanizates. Part IV. Unfilled vulcanizates, J. Appl. Polym. Sci. 10 (8) (1966) 1203–1211.
[77] J.S. Bergström, M.C. Boyce, Constitutive modeling of the large strain time-dependent behavior of elastomers, J. Mech. Phys. Solids 46 (5) (1998) 931–954.
[78] Y. Qi, J. Caillard, R. Long, Fracture toughness of soft materials with rate-independent hysteresis, J. Mech. Phys. Solids 118 (2018) 341–364.
[79] Z.J. Wang, C.P. Xiang, X. Yao, P. Le Floch, J. Mendez, Z.G. Suo, Stretchable materials of high toughness and low hysteresis, Proc. Natl. Acad. Sci. U. S. A. 116 (13) (2019) 5967–5972.
[80] J. Liu, C. Yang, T. Yin, Z. Wang, S. Qu, Z. Suo, Polyacrylamide hydrogels. II. Elastic dissipater, J. Mech. Phys. Solids 133 (2019) 103737.
[81] Griffith, A.A. The theory of rupture. Proceedings of the First International Congress for Applied Mechanics, Delft, 1924, (Biezeno, C. B; Burgers, J. M.), 55.
[82] B. Lawn, Fracture of Brittle Solids, Cambridge University, 1975.
[83] A. Thomas, The development of fracture mechanics for elastomers, Rubber Chem. Technol. 67 (3) (1994) 50–67.